Full Text View

Volume 30, Issue 2 (February 2000)

Journal of Physical Oceanography
Article: pp. 402–415 | Abstract | PDF (2.64M)

Examination of the Impact of a Coupled Atmospheric and Ocean Wave System. Part II: Ocean Wave Aspects

R. Lalbeharry

Recherche en Prévision Numérique, Atmospheric Environment Service, Downsview, Ontario, Canada

J. Mailhot, S. Desjardins, and L. Wilson

Recherche en Prévision Numérique, Atmospheric Environment Service, Dorval, Quebec, Canada

(Manuscript received July 27, 1998, in final form April 8, 1999)

DOI: 10.1175/1520-0485(2000)030<0402:EOTIOA>2.0.CO;2

ABSTRACT

A coupled atmospheric and ocean wave system has been developed to study the impact of changes of surface roughness length induced by ocean waves. A two-way coupling between a mesoscale atmospheric model, MC2, and an oceanic wave model, a regional version of WAM Cycle-4, was designed to ensure consistency in the treatment of the atmospheric boundary layer parameterizations between the two models. Two different approaches, based on the wave age of Smith et al. and the wave-induced stress of Janssen, are used to compute a coupling parameter, called the Charnock parameter, expressed as the nondimensional surface roughness length. The coupling between the two models is accomplished by the use of this parameter, which is a function of sea state, instead of the constant value obtained from empirical studies using the well-known Charnock relation.

The impacts on the atmospheric forecasts are discussed in Part I. In Part II, the ocean wave forecasts resulting from this two-way coupling are discussed for four different real cases. The two approaches are evaluated by comparing ocean wave model outputs obtained from the coupled and uncoupled systems against buoy observations. The coupling has some beneficial impact, especially in areas of extreme sea states. The significant wave heights are reduced in the coupled runs and generally show better agreement with the buoy observations. The impact of the coupling also exhibits some dependence on the intensity of the cyclone development, with larger changes occurring in the case of rapidly deepening storms.

1. Introduction

In Part I of this study (Desjardins et al. 2000, hereinafter referred to as DML), the impact on the atmosphere of two-way coupling of a mesoscale atmospheric model and the wave model WAM was investigated and described. The results of tests on four storm cases showed that the impacts were small in terms of the evolution of the storm itself, but that locally large impacts on some of the surface parameters were noted. In Part II we investigate and describe the impact of the coupling on the evolution of the surface ocean wave field.

The development of the third generation (3G) wave model called WAM described in The WAMDI Group (1988) has led to a gradual replacement of earlier 1G and 2G wave models in most but not all deep water prediction systems since 1988. The current Cycle-4 version of WAM (hereinafter referred as WAM4) is based on the ideas of Janssen (1991) in which the winds and waves are coupled; that is, there is feedback of growing waves on the wind profile. The effect of this feedback is to enhance the wave growth of younger wind seas over that of older wind seas for the same wind. This results in the drag of airflow over oceans to be sea state dependent in agreement with the findings by Donelan (1982), Maat et al. (1991), Smith et al. (1992), Donelan et al. (1993), and Johnson et al. (1998). The evidence from these studies also suggests that the normalized sea surface roughness is strongly dependent on the sea state, that is, on the stage of wave development or wave age. This lends support for the development of a coupled atmosphere–ocean wave prediction system.

Global and regional versions of WAM4 have been implemented in operational mode at various national wave forecast centers such as the European Centre for Medium-Range Weather Forecasts (ECMWF), the U.S. Fleet Numerical Meteorology and Oceanography Center (FNMOC), the U.S. National Centers for Environmental Prediction (NCEP), and the Atmospheric Environment Service (AES) of Canada using different spatial and spectral resolutions. Validation studies (Wittmann et al. 1995; Cardone et al. 1996; Khandekar and Lalbeharry 1996; Janssen et al. 1997; Bidlot et al. 1998) on the performance of WAM4 against buoy observations indicate that the analyzed wave heights generated by WAM4 are of good quality and in good agreement with the buoy observations, while the quality of the wave forecasts shows a slow deterioration with time.

Previous coupling studies (Weber et al. 1993; Janssen 1994; Doyle 1995; Janssen and Viterbo 1996; Lionello et al. 1998) have tended to indicate that the impact of coupling on the sea state may be greater than the impact on the atmosphere. For example, Janssen (1994) and Janssen and Viterbo (1996), using a version of WAM4 with a T63 version of the ECMWF model, concluded that the sea state dependence of momentum transfer had a definite impact on the wave climate with a general reduction on the order of 10% of the wave heights in the coupled runs. The studies by Doyle (1995) and Lionello et al. (1998) both used coupled simulations of idealized cases of midlatitude cyclones. Doyle (1995) found that the high wind speeds generated in the vicinity of a marine cyclone result in a substantial growth of surface ocean waves, especially along the warm front and to the rear of the cyclone, with maximum significant wave heights (SWH) exceeding 12 m. The locations of the SWH maxima are linked to the local surface wind speed maxima, as in the simulations of Weber et al. (1993). Lionello et al. (1998) noted that the two-way coupling significantly decreases the SWH and the surface wind speed. The impact is larger for extreme storms but is also clearly seen for weaker cyclones and results in a reduction of the maximum SWH varying between 15% and 20%, depending on the intensity of the idealized storm.

Part II of this study continues the investigation of the impact of two-way interaction in the simulation of four real storm cases. The reader is referred to DML for detailed descriptions of the atmospheric model and the storm evolution, for a description of the coupling procedure for model integration, and for a discussion of the impact on the atmospheric parameters. This part concentrates on the wave model, gives a more complete description of the coupling parameters used (section 2), and describes the impact of the coupling on the wave simulations (section 3). A summary and conclusions are presented in section 4.

2. Coupled atmosphere–ocean wave model system

a. Numerical models

The coupled model system consists of the atmospheric model called MC2 (Mesoscale Compressible Community model: Benoit et al. 1997) as described in DML and a regional version of the ocean surface wave model WAM4 (The WAMDI Group 1988; Komen et al. 1994). The WAM4 grid is shown in Fig. 1 of DML and is not repeated here. It lies well inside the MC2 model grid and extends from 25° to 70°N, 80° to 25°W in the North Atlantic with a grid spacing of 0.5° in both latitude and longitude directions.

The WAM4 describes the evolution of the directional spectrum $E(f, \theta, \Phi, \lambda, t)$ of waves in deep water by solving the wave energy transfer equation for 25 frequencies logarithmically spaced from 0.042 to 0.41 Hz at intervals of $\Delta f/f = 0.1$ and 24 direction bands of 15° each. Here f is frequency, θ is wave direction, Φ is latitude, λ is longitude, and t is time. The wave spectrum is locally modified by the net source term $S = S_{in} + S_{nl} + S_{ds}$, where S_{in} represents the wind energy input, S_{nl}

represents the nonlinear wave–wave interaction energy redistribution approximated by the discrete interaction approximation (Hasselmann et al. 1985), and S_{ds} is energy dissipation due to whitecapping.

WAM4, as used in this project, is modified from the version of the model described in WAMDI Group (1988) in several ways. First, S_{in} is based on the quasilinear theory of wave generation of Janssen (1991). Janssen's theory implies a one-way coupling of the wave growth to the atmospheric boundary layer and results in a higher growth rate than the original Snyder et al. (1981) scheme (Bender 1996). To compensate for this higher growth rate in WAM4, Janssen (1991) modified S_{ds} to include an additional term proportional to the square (fourth power) of the wavenumber (frequency). Second, our version of the model also includes a linear growth term in S_{in}, following Cavaleri and Malanotte-Rizzoli (1981), but with a filter to eliminate contributions from frequencies lower than the Pierson–Moskowitz frequency (Tolman 1992). Third, the portion of the spectrum beyond the high frequency limit f_{hf} of the prognostic region is modeled assuming the energy varies as f^{-5} and assuming the same directional distribution as for the last band of the prognostic portion of the spectrum. A diagnostic tail for $f > f_{hf}$ is necessary to compute the nonlinear transfer in the prognostic region and the integral quantities in the dissipation function.

The net source term is integrated using a semi-implicit time integration scheme. To avoid instabilities in the source term integration in the high frequency portion of the spectrum, a limiter was used, following Hersbach and Janssen (1999). Numerical oscillations developed in the high frequency part of the spectrum in certain circumstances are suppressed by replacing the semi-implicit integration scheme with a fully implicit scheme. The propagation scheme used is upwind first order and is inherently diffusive. In the present study, the propagation time step was set to 300 s, the source term integration time step was set to 300 s, and the minimum grid spacing is about 20 km. In deep water, the maximum group velocity $C_{g\max} = 19.5$ m s^{-1} for the highest frequency waves of 0.042 Hz so that the CFL criterion for numerical stability is more than adequately satisfied.

b. Coupling parameter

In both atmospheric and ocean-wave models the sea surface roughness length z_0 is given by the Charnock equation (Charnock 1955) in terms of u_* and the acceleration due to gravity g as

$$z_0 = \beta u_*^2/g, \quad (1)$$

where u_* is the friction velocity and the Charnock parameter β is dependent on the sea state. Wu (1980) suggested a constant value $\beta_{CH} = 0.0185$ based on a wide range of datasets. More recent studies have attempted to parameterize the Charnock parameter in terms of the sea state (Donelan 1982; Huang 1986; Toba et al. 1990; Nordeng 1991; Maat et al. 1991; Janssen 1991; Smith et al. 1992; Donelan et al. 1993). In the formulation of Janssen (1991), β is modified to include the wave-induced stress for mixed sea and swell situations; that is,

$$\beta_{WS} = \alpha/\sqrt{\{1 - (\tau_w/\tau)\}}, \quad (2)$$

where α is a tuned constant set equal to 0.01 and the sea state dependence is reflected through the wave-induced kinematic stress τ_w, obtained from the integration of the model wind input source term over all frequencies and directions. In (2) the total kinematic stress $\tau = \tau_a + \tau_w$, where τ_a is the atmospheric turbulent kinematic stress from flow over a rigid flat surface.

In the formulation of Smith et al. (1992) using the HEXOS dataset, β is modified to include the wind sea parameter called wave age, $\tilde{\xi} = c_p/u_*$, for pure wind sea; that is,

$$\beta_{WA} = 0.48/\tilde{\xi}, \quad (3)$$

where c_p is the phase speed of the peak of the spectrum. Other relations between z_0 and the wave age have been proposed in various studies (e.g., Maat et al. 1991; Nordeng 1991), but here the Smith et al. relation will be used (see Perrie and Wang 1995 for further discussion).

The 10-m level drag coefficient under neutral conditions is given by

$$C_D = u^2_*/u^2_{10}, \quad (4)$$

where u_{10} is the neutral 10-m level wind given by

$$u_{10} = (u_*/\kappa)\ \ln(10/z_0) \quad (5)$$

in which $\kappa = 0.41$ is the von Kármán constant. From (4) and (5)

$$z_0 = 10 \exp(-\kappa/\sqrt{C_D}), \quad (6)$$

and from (1) the nondimensional roughness length or the Charnock parameter

$$\beta_{WS} = g z_{0WS}/u^2_{*WS} \quad \text{or} \quad \beta_{WA} = g z_{0WA}/u^2_{*WA}. \quad (7)$$

Here, the subscripts "WS" and "WA" refer, respectively, to parameters based on the formulation of Janssen (1991) and that of Smith et al. (1992). Using (1) and (5) it can be shown (see the appendix in DML) that

$$\Delta u_{10}/u_{10} = (\Delta u_*/u_*)[1 - 2\sqrt{C_D}/\kappa] - (\Delta\beta/\beta)\sqrt{C_D}/\kappa, \quad (8)$$

where the ratio $\Delta x/x$ is defined as (coupled x − uncoupled x)/uncoupled x so that $\Delta\beta/\beta = (\beta - \beta_{CH})/\beta_{CH}$ with $\beta_{CH} = 0.018$. The MC2 model uses the β provided by WAM4 in the coupled mode and β_{CH} in the uncoupled mode to obtain its own u_* and u_{10} using its own boundary layer physics. The resultant u_{10} passed to the WAM4 includes the atmospheric stability, but the WAM4 considers this u_{10} to be the equivalent neutral wind, that is, the wind that produces the same surface stress as the actual 10-m level wind. Hence, the u_* as obtained by the MC2 model is based on the actual wind, while the u_* obtained by the WAM4 is based on the equivalent neutral wind and these two u_* must be consistent in the MC2 model and the WAM4 boundary layer formulations. In (8) $(C_D)^{1/2}/\kappa \approx 0.12$ and relative changes to u_{10} are due to contributions from the relative changes to both u_* and β with respect to the state based on β_{CH}. A positive (negative) change in β and negative (positive) change in u_* contributes to the decrease (increase) of u_{10}.

Given u_{10} and τ_w, (5) can be solved for u_* iteratively. Now C_D is obtained from (4), z_0 from (6), and β_{WS} from (7). Given u_{10} and c_p, the various parameters obtained using wave-induced stress can be similarly obtained using wave age. The ocean wave model WAM4 is coupled to the atmospheric model MC2 through the coupling parameter β_{WS} based on wave-induced stress or β_{WA} based on wave age. The results of the experimental runs presented in section 3 are based on these two formulations of the coupling parameter, which is passed to the MC2 model as described in the paragraph below.

c. Marching procedure

The time marching procedure is described in detail in DML. In summary, for each 1800 s coupling interval, the wave model uses winds from the atmospheric model valid at the beginning of the previous interval (1800 s old) for the first half (900 s) and winds valid at the beginning of the current interval for the last half to generate the β field at the end of the current interval for exchange with the MC2 model. The 1800 s coupling interval chosen here is the optimal interval based on tests using different coupling intervals to allow the β field to adjust so that it generally lies in the acceptable range of 0.01 to 0.1. The values of β (β_{WS} and β_{WA}) so computed by the wave model are then passed to the atmospheric model for use in the next step. Effectively, this means that both models are using slightly "old" information in their computations, but it allows them to be integrated simultaneously, avoiding the necessity for either model to wait for the other. Since the coupling interval corresponds to 6–300 s time steps of the wave model, it is the β values computed every six WAM4 time steps that are passed to the MC2 model.

d. Simulation strategy

Following the notation introduced in Part I, the model simulations are done in a control (or uncoupled) mode referred to as CH [for β = const in (1)] and in a two-way coupled mode referred to as WS and WA, for wave-induced stress and wave

age, respectively. An uncoupled run is a one-way interaction run in which the MC2 model uses a constant value of β_{CH} = 0.018 over the entire MC2 model grid and provides the resulting 10-m wind fields to WAM4, but the wave model uses the wave-induced stress, or wave age, formulation for β. In a coupled run the MC2 model receives from the WAM4 the sea-state-dependent parameter β, and the WAM4, in return, receives from the MC2 model the 10-m level wind field generated using the β provided by the wave model in the previous exchange. For the wave model Perrie and Wang (1995) showed that in one-way wind–wave interaction using the Snyder et al. wind input term of WAM3 and the Janssen wind input term of WAM4 both have the ability to generate higher SWH in closer agreement with observations than the SWH based on no wind–wave coupling but with the latter having a higher growth rate than that of the former as pointed out also by Bender (1996).

The three phases of the simulation of each storm case are described in detail in DML, while details on the numerical experiments and period covered for each case are given in Tables 1 and 2, also in DML. Suffice to say here that in the spinup run the WAM4 starts from a flat sea (cold start). This run is done only once and is based on the wave-induced stress. It provides the same initial sea state to be used as input to all transition runs in warm start. The initial sea state for the evaluation run in warm start is different for each run in this phase. Note that when the coupled system is in control mode, the surface roughness length parameterization in the wave model is based on WS.

For each of the four real storm cases, the WAM4 results obtained in the evaluation phases from the two-way interaction were compared against those from the control run (one-way interaction). Results from all runs were also compared against observations from the buoys listed in Table 1 (see also Fig. 1 of DML for buoy identification and location) to give a measure of the impact of the coupled model system. As a first step in the study of the impact of a coupled model system, only validation of the results against buoy observations was considered. In future studies, it might be useful to consider detailed comparisons against remote sensing data as well. For the superstorm and Hurricane Luis the results were also compared against the results generated by the WAM4 running in a hindcast mode and driven by winds obtained from a man-machine-mix (MMM) analysis procedure that used all conventional meteorological data, including ship and buoy observations too late for use in real time (Cardone et al. 1996). The MMM wind field was produced at hourly intervals for the transition and evaluation periods on a 0.5° lat × 0.5° long grid over the area covered by the WAM with the same grid resolution as the MMM winds for these two storms and are considered to be the best obtainable winds. All four storms studied generated extreme sea states. Extreme measured significant wave heights (SWH) were 16 m (superstorm at buoy 44137 at 0000 UTC 15 March 1993) and more than 17 m (Luis at buoy 44141 at 0000 UTC 11 September 1995).

3. Results of one-way and two-way interactions of the coupled model system

a. The Superstorm of March 1993

Figure 1 shows time series plots of observed and model-generated significant wave heights in coupled (WS and WA) and uncoupled (CH) modes at four buoy locations in the Scotian Shelf region during the evaluation period. The model shows a general tendency to overpredict the SWH, with greater overprediction in uncoupled mode. Both couplings (WS and WA) reduce the SWH compared to the CH run, in agreement with the findings of previous studies (e.g., Janssen and Viterbo 1996; Lionello et al. 1998). This results in improved agreement between the observed and model-generated SWH. Note that the WS and WA couplings give very similar results, with slightly larger SWH in the WA runs than in the WS run. Also shown is the SWH generated using the MMM winds in a hindcast mode. The SWH based on the MMM winds is in better agreement with the observed SWH than those in the coupled and uncoupled runs. This better agreement can be ascribed to the fact that the MMM winds resolved the finescale structure of the wind field including two well-defined surface jet streaks that passed over the buoy array of the U.S. and Canada east coast (Cardone et al. 1996).

Figure 2 gives a snapshot of the SWH in meters based on WS (left panel) and WA (right panel) at 1200 UTC 14 March 1993. It can be seen that the SWH in coupled modes is lower than the SWH in uncoupled mode by 1–3 m using either WS or WA. The area of reduction of SWH is in good agreement with the reduction in the MC2 model winds in the coupled mode (see Fig. 4 in DML) and lies mainly in the area of extreme sea states.

Figure 3 shows the 24-h forecast of the WAM-generated Charnock parameter difference (with respect to a constant value of 0.018) for the WS and WA runs, valid at the same time as Fig. 2. The vector wind field provided by the MC2 model to the WAM in the coupled mode is superimposed in meteorological convention with full barbs representing 10 m s^{-1} and half barbs 5 m s^{-1}. In the region to the southeast of Newfoundland the more rapid change in wind speed (see Fig. 4 in DML) and wind direction gives rise to relatively larger values of β for the WS run (left panel) and the WA run (right panel), that is, younger waves. In general, β is larger for WS than WA, indicating that the sea states generated using τ_w are younger and rougher than those generated using ξ. Figure 3 also shows that the Charnock parameter β is in general larger than 0.018 over most of the domain. A comparison with Fig. 3 in DML indicates that the impact of coupling is to increase the surface roughness z_0 where younger waves are generated. When the coupling parameter β given by WAM is larger than 0.018 (younger and rougher seas), the resulting winds provided by the MC2 model are lighter than those in the

CH run with a consequent reduction in the SWH generated. The reverse is true if the β is less than 0.018 (older and smoother seas). A value of $\beta = 0.018$ everywhere is considered a mean value representative of the various stages of the wave field development (Lionello et al. 1998). The area of small β just southwest of Nova Scotia lies in an area of predominantly swells and mainly in the same area with $z_0 \leqslant 1$ mm as shown in Fig. 3 in DML for both coupled and uncoupled simulations. The areas of maxima of β for WS and WA match closely those corresponding to the drag coefficients (not shown). An examination of the drag coefficient in the coupled model indicates that $C_D > 3 \times 10^{-3}$ lies in a region of wind speed in excess of 20 m s^{-1} (see Fig. 4, DML) and that the C_D due to wave age is almost the same as that due to wave-induced stress. Thus, as the wind speed increases, the difference in drag coefficients between the pure wind sea and the mixed wind sea/swell decreases, which agrees with Donelan et al. (1997).

For the four cases studied it was generally found that the differences using either WS or WA are rather small but the impact is a little larger with the WS formulation. Therefore, only the results based on WS will be presented in the rest of this paper.

b. The storm of March 1986

The second case selected is the COMPARE I storm as described in DML. The results presented here are from the 24-h forecast valid at 1200 UTC 7 March 1986, the time at which the minimum central pressure was reached. A comparison of the coupled $u*$ based on the equivalent neutral wind (grayscale area in Fig. 4) with the $u*$ based on the actual wind (dashed line in Fig. 7a in DML) indicates the two $u*$ fields are nearly equal, giving confidence that the boundary layer formulations of the surface stress fields of the MC2 and WAM4 models are indeed consistent. Figure 4 also shows a good correlation between the $u*$ and the neutral drag coefficient C_D.

Another feature of Fig. 7a in DML is that $\Delta u*$ (the difference between WS and CH) is positive over most of the area. There is a narrow band of negative $\Delta u*$ just behind the cold front in the predominantly swell area. The same is true for $\Delta\beta$ in Fig. 5a (grayscale area), that is, increase (decrease) in $\Delta\beta$ is associated with increase (decrease) in $\Delta u*$ so that the impact of one is to reduce the impact of the other on u_{10}, the 10-m winds. It can be seen from (8) that for $\Delta\beta$ close to zero ($\beta \sim 0.018$), changes in u_{10} depend on changes in $u*$ only. Negative values of $\Delta\beta$ are always close to zero since the minimum value of β is 0.01. However, the second term in (8) is the dominant term, especially in areas of large positive $\Delta\beta$, so that the sign of u_{10} is governed to a large extent by the sign of $\Delta\beta$. In the area inside the 20 m s^{-1} isotach (Fig. 5b) $\Delta\beta$ is largely positive and is the dominant factor in reducing the jet intensity by 1–3 m s^{-1}. This results in a reduction of SWH of 1–2 m (Fig. 5c). The area of maximum reduction lies mainly in the area of extreme sea state generated by the southerly jet streak with maximum intensity close to 24 m s^{-1}. In the swell-dominated area just behind the cold front, $\Delta\beta$ is close to zero, while $\Delta u*$ is largely negative so that the reduction in u_{10} is due mainly to the reduction in $u*$ in the coupled mode. Outside the area bounded by the 16 m s^{-1} isotach, the impact of changes in $u*$ on u_{10} in the coupled mode is rather small, which resulted also in negligibly small impact on the coupled SWH field. For significant impact to occur it is imperative that β be much larger than the mean sea state as given by the Charnock constant of 0.018 in areas of extreme sea state. Although the sea state generated by this storm was locally high, it was less so than for the March 1993 storm. Therefore, the impact of coupling in terms of SWH differences is generally larger for the superstorm than for the COMPARE I case.

c. The "Bomb" of February 1995

The February 1995 storm, hereinafter called the "bomb," also underwent explosive cyclogenesis with the central pressure falling by 20 mb in 12 hours and reaching 973 mb at 0000 UTC 5 February 1995. This storm had a well-defined low-level jet extending from the surface to about 700 mb, which is discussed in DML. The previous two cases demonstrated that significant impact on the wind field in the coupled model system is associated with large changes of β from the mean sea state, especially in areas of extreme sea state. A sensitivity test was conducted using this case. An additional run was carried out (designated "5WS") in which the β obtained from WAM was multiplied by a factor of 5 in regions where β exceeds 0.036. That is, the sea in these regions is artificially forced to appear younger and hence rougher as seen by MC2.

Figure 6 shows the time series plots of the SWH generated using the MC2 model winds from the CH, WS, and 5WS runs, compared to observations at buoys 41001 and 44005 for the simulation period 4–6 February. At buoy 41001 the model sea state is moderate and close to the observed sea state. The differences in SWH between CH and WS runs are small. However, the 5WS run clearly underpredicts the SWH, at least until 1200 UTC 5 February. At buoy 44005 the observed sea state is still moderate, while the model sea state is more extreme with large overprediction of the SWH shown by the CH run. In this case the MC2 wind from the 5WS run did a better job than winds from the WS run in reducing significantly the

SWH. As discussed in DML, the artificial enhancement (by a factor of 5) of β occurs between 1000 and 1800 UTC 4 February 1995 for buoy 41001 and between 1600 UTC 4 February and 0400 UTC 5 February for buoy 44005 when the storm is in its rapid development phase. These periods correspond well in Fig. 6 with the time when the SWH changes rapidly between runs WS and 5WS. During these periods, the enhanced Charnock parameter in the atmospheric model results in reduced wind speeds (Fig. 9 in DML) and, therefore, in decreased SWH in the wave model. Differences in SWH at later times can be attributed to swells originating from the south and generated with differing wind conditions, especially for buoy 44005 after 0400 UTC 5 February.

Figure 7 shows the 24-h forecast valid at 0000 UTC 5 February of WAM-generated SWH and u_* in the coupled mode. It is seen that, in general, the SWHs are smaller with 5WS than WS and that the impact of the enhanced β on the SWH is largest in the area of extreme model sea state. The enhanced β causes a reduction of the MC2 model wind (see Fig. 10 in DML) which in turn causes a reduction in the WAM-derived u_* as seen in Fig. 7b with maximum reduction in the southeast quadrant of the low pressure system. It can be surmised from this sensitivity study that the younger and rougher seas are quite effective in reducing the overprediction of the SWH in areas of extreme sea state, while in areas of moderate seas the effect of coupling is minimal and may even degrade the results.

d. Hurricane Luis of September 1995

The fourth case studied is Hurricane Luis whose trajectory during the simulation period is shown in Fig. 12 in DML. As Luis crossed the Canadian Atlantic, it gradually acquired extratropical characteristics and generated 30-m maximum waves near the continental shelf with SWH in excess of 17 m as observed by buoy 44141. Because of the mesoscale and convective nature of a hurricane, the MC2 model was used to produce winds at 50-km and 25-km resolutions, using a variety of convection schemes in an attempt to maximize the effect of the convection on the intensification and propagation of the storm. The winds at these two MC2 model grid resolutions were then interpolated onto the 0.5° lat × 0.5° long grid for driving the WAM4 in both coupled and uncoupled modes.

Figure 8 shows time series plots of SWH at buoy 44141 for the 36-h evaluation period 0000 UTC 10 September to 1200 UTC 11 September for the two MC2 grid resolutions. The MMM winds were produced on a 0.5° lat × 0.5° long grid over the area covered by the WAM4 with the same grid resolution as the MMM winds. Driven by the MMM winds, the WAM4 was capable of generating SWH values close to 17 m at buoy 44141. Using winds from MC2, the sea states at buoy 44141 were grossly underpredicted, reaching SWH values of 9–10 m only. The maximum SWH is also delayed by about 3 hours with the model winds. The coupling in this case slightly degraded the results since the impact of coupling is to reduce further the SWH already underpredicted in areas where the sea state is rougher than that based on the Charnock constant of 0.018. Also, the benefit gained in the estimation of SWH by using the 25-km resolution MC2 model grid compared to the 50-km grid is marginal. The results that follow are for runs based on the 25-km resolution only.

Figure 9 displays the 24-h forecast/hindcast of the SWH (Fig. 9a) and the u_{10} (Fig. 9b) fields valid 0000 UTC 11 September 1995, the time at which the maximum wave height was observed at buoy 44141. At this time, the surface jet streak in the MMM winds had a maximum intensity around 32 m s^{-1}, while that of the coupled u_{10} was around 23 m s^{-1} and out of phase with the MMM wind jet streak. This resulted in the out-of-phase relationship and the underforecasting of the coupled SWH when compared with the SWH based on MMM winds, results that are confirmed also by the time series plots in Fig. 8. The results suggest that the WAM4 is capable of generating a 17-m wave given high quality winds as the MMM winds and if the small-scale intense surface wind maxima or jet streak phenomena with high spatial coherency associated with intense storms can be resolved in operational analysis and forecast system (Cardone et al. 1996). The tendency of WAM4 is to underpredict the most extreme sea states, and the overall effect of coupling is to dampen both the atmospheric and wave fields. Coupling, therefore, would hinder the performance of the wave model in the generation of the peak SWH in extreme storm events. However, if the driving winds contain errors that lead to overprediction of the SWH including the peak SWH, then a coupled model system would improve the performance of the wave model.

Figure 10 documents the modeled peak wave period with the wind field superimposed, valid at 0000 UTC 11 September. Figure 10a shows the results with the MMM wind field, while Fig. 10b is for the coupled WS run. The observed peak period at buoy 44141 at this time is close to 18 sec, giving a group velocity of the ocean wave system moving to the northeast of about 15 m s^{-1}. The corresponding peak period and group velocity of the waves generated using the MMM winds are 17 sec and 13.5 m s^{-1}, respectively, and those based on the coupled model system close to 10.0 sec and 8.0 m s^{-1}, respectively, in the vicinity of buoy 44141. The mean observed and modeled northeastward motions of the storm for the period 0000 UTC 10 September to 0000 UTC 11 September are both close to 15 m s^{-1}. Thus, the observed ocean wave system and the storm are both moving with nearly the same speed and in the same direction. This is also true in the MMM wind simulation. As a result, the wave system is trapped, experiencing unlimited growth in the process. However, in the runs with the coupled model winds, the Hurricane Luis forward speed toward the northeast is faster than that of the waves it generated. Consequently, the coupled model waves are untrapped and left behind as swells. After 0000 UTC 11

September, Luis accelerated rapidly reaching a forward speed to the northeast of about 26 m s^{-1}, thus ending the unlimited growth of waves. The failure to correctly simulate the trapping effect could at least partially account for the lack of agreement between the SWH based on MMM winds and the coupled SWH at buoy 44141 and the inability of the coupled runs to correctly simulate the extreme observed sea states.

The impact of coupling is also rather minimal in the case of Luis, as shown in Fig. 11. Figure 11a shows $\Delta\beta$, the SWH differences (coupled − uncoupled) and the coupled swell heights. Figure 11b indicates Δu_* (coupled − uncoupled) with the coupled vector wind field superimposed. It is assumed that the u_* derived by the WAM4 using the MC2 model uncoupled u_{10} is a reasonable representation of the MC2 model uncoupled u_*, as mentioned above with regard to the COMPARE I case (cf. Fig. 4). In the eastern quadrant of Luis in the area of the southerly jet streak $\Delta\beta$ is positive, while Δu_* is negative. According to (8) both terms contribute to reduce u_{10} by 1–2 m s^{-1}, which in turn reduces the SWH by 1–2 m over a very small area. Normally, for a fully developed sea, the SWH is proportional to the square of u_{10} (e.g., SWAMP Group 1985, p. 24), and therefore a 10% relative change in u_{10} would lead to a 20% relative change in SWH. In the southwest quadrant in the area of the northerly jet streak, $\Delta\beta$ is small but negative due to the predominance of swells, while Δu_* is positive and is the dominant term. In this case both terms contribute to increase u_{10} by 2–3 m s^{-1} (about 10%, see Fig. 13 in DML) resulting in an increase of SWH less than 1 m over a small area, smaller than would be expected. This small SWH increase may be ascribed to the fact that this area consists mainly of swells left behind by the faster-moving Luis and that the fetch conditions are changing too rapidly for the waves to adjust to the wind changes; that is, the sea has not had a chance to become well developed.

4. Summary and conclusions

In this study the impact of coupled atmospheric–ocean wave models was examined in the context of mesoscale short-term forecasts with real cases of rapidly developing storms, thus extending previous studies on idealized cases. It should be emphasized here that the results obtained in this study are valid for the temporal scale ~ 2 days and a spatial scale in the mesoscale category. The impact of coupling, however, may be more significant for larger temporal and spatial scales (e.g., Janssen and Viterbo 1996). Part II of the present work has focused on the impact of the coupling on significant wave heights and peak periods as estimated by WAM4.

Four cases having different development were simulated, covering a wide spectrum of sea state conditions in the midlatitudes. Part I of this study (DML) showed that the most significant impact of the coupling was found in the 10-m wind speeds where a reduction of about 10% occurred in association with enhanced surface roughness lengths due to the presence of younger and rougher seas. The decrease in the surface wind translated into a reduction of the significant wave heights, but the sea state was not significantly altered. Comparison with observations suggests that the impact is beneficial, especially in areas of extreme sea states where the coupling tended to reduce overestimation of the SWH. The impact of the coupling also exhibits some dependence on the intensity of the cyclone development, indicating significantly larger changes in the vicinity of rapidly deepening storms. This result is consistent with the results of Lionello et al. (1998) for idealized cases.

The generation of extreme sea states, as in the case of Hurricane Luis, needs high quality winds and the resolution of the mesoscale surface jet streak phenomena, normally associated with intense storms, with high spatial coherency in operational analysis and forecast system. The poor simulation of Hurricane Luis demonstrates the need for more accurate specification of an operationally produced wind field that drives the wave model in the prediction of extreme sea states in storm events.

Younger waves are generated where the winds undergo changes in both speed and direction. This is particularly true at the leading edge of an advancing or developing storm as exhibited by the case of the Superstorm of March 1993. A crucial factor also in extreme wave generation is the presence of a well-defined surface jet with spatial and temporal continuity in the storm. Here, the coupling produced the greatest impact as demonstrated in the superstorm and COMPARE I cases.

Acknowledgments

The authors are grateful to Bechara Toulany and Dr. Will Perrie of the Bedford Institute of Oceanography for providing some components of the computer code relating to wave age; to Ralph Bigio of the Meteorology and Oceanography Centre, Halifax, Nova Scotia, for making available the buoy data for Hurricane Luis; to Bridget Thomas of the Climate Research Branch, Bedford, Nova Scotia, for providing the buoy data for the March 1993 storm; and to Yves Chartier and Vivian Lee of Recherche en Prévision Numérique for valuable computer assistance. We acknowledge suggestions for improvements by the reviewers.

REFERENCES

Bender, L. C., 1996: Modification of the physics and numerics in a third-generation ocean wave model. *J. Atmos. Oceanic Technol.*, **13,** 726–750..

Benoit, R., M. Desgagné, P. Pellerin, S. Pellerin, Y. Chartier, and S. Desjardins, 1997: The Canadian MC2: A semi-Lagrangian, semi-implicit wide band atmospheric model suited for fine-scale process studies and simulation. *Mon. Wea. Rev.*, **125,** 1726–1750.. Find this article online

Bidlot, J. R., M. Holt, P. A. Wittmann, R. Lalbeharry, and H. S. Chen, 1998: Towards a systematic verification of operational wave models. *Proc. Third Int. Symp. on WAVES'97,* Virginia Beach, VA, American Society of Engineers, 653–667..

Cardone, V. J., R. E. Jensen, D. T. Resio, V. R. Swail, and A. T. Cox, 1996: Evaluation of comtemporary ocean wave models in rare extreme events: The "Halloween storm" of October 1991 and the "Storm of the Century" of March 1993. *J. Atmos. Oceanic Technol.*, **13,** 198–230..

Cavaleri, L., and P. Malanotte-Rizzoli, 1981: Wind wave prediction in shallow water: Theory and applications. *J. Geophys. Res.*, **86,** 10 961–10 973..

Charnock, H., 1955: Wind stress on a water surface. *Quart. J. Roy. Meteor. Soc.*, **81,** 639–640..

Desjardins, S., J. Mailhot, and R. Lalbeharry, 2000: Examination of the impact of a coupled atmospheric and ocean wave system. Part I: Atmospheric aspects. *J. Phys. Oceanogr.*, **30,** 385–401.. Find this article online

Donelan, M. A., 1982: The dependence of the aerodynamic drag coefficient on wave parameters. *Proc. First Int. Conf. on Meteorology and Air–Sea Interaction of the Coastal Zone.* The Hague, Netherlands, Amer. Meteor. Soc., 381–387..

— ~~,~~F. W. Dobson, S. D. Smith, and R. J. Anderson, 1993: On the dependence of sea surface roughness on wave development. *J. Phys. Oceanogr.*, **23,** 2143–2149.. Find this article online

— ~~,~~W. Drennan, and K. B. Katsaros, 1997: The air–sea momentum flux in conditions of wind sea and swell. *J. Phys. Oceanogr.*, **27,** 2087–2099.. Find this article online

Doyle, J. D., 1995: Coupled ocean wave/atmosphere mesoscale model simulations cyclogenesis. *Tellus,* **47A,** 766–778..

Hasselmann, S., K. Hasselmann, J. H. Allender, and T. P. Barnett, 1985: Computations and parameterizations of the nonlinear energy transfer in a gravity-wave spectrum. Part II: Parameterizations of the nonlinear energy transfer for application in wave models. *J. Phys. Oceanogr.*, **15,** 1378–1391.. Find this article online

Hersbach, H., and P. A. E. M. Janssen, 1999: Improvement of the short-fetch behavior in the Wave Ocean Model (WAM). *J. Atmos. Oceanic Technol.*, **16,** 884–892..

Huang, N. E., 1986: A study of the relationship among wind speed, sea state, and the drag coefficient for a developing wave field. *J. Geophys. Res.*, **91,** 7733–7742..

Janssen, P. A. E. M., 1991: Quasi-linear theory for wind wave generation applied to wave forecasting. *J. Phys. Oceanogr.*, **21,** 1631–1642.. Find this article online

— ~~,~~1994: Results with a coupled wind wave model. ECMWF Tech. Rep. No. 71, 60 pp. [Available from ECMWF, Shinfield Park, Reading, Berkshire RG2 9AX, United Kingdom.].

— ~~,~~and P. Viterbo, 1996: Ocean waves and the atmospheric climate. *J. Climate,* **9,** 1269–1287.. Find this article online

— ~~,~~B. Hansen, and J. R. Bidlot, 1997: Verification of the ECMWF wave forecasting system against buoy and altimeter data. *Wea. Forecasting*, **12,** 763–784.. Find this article online

Johnson, H. K., J. Holstrup, H. J. Vested, and S. E. Larsen, 1998: On the dependence of sea surface roughness on wind waves. *J. Phys. Oceanogr.*, **28,** 1702–1716.. Find this article online

Khandekar, M. L., and R. Lalbeharry, 1996: An evaluation of Environment Canada's operational wave model based on moored buoy data. *Wea. Forecasting*, **11,** 139–152.. Find this article online

Komen, G. J., L. Caveleri, M. Donelan, K. Hasselmann, S. Hasselmann, and P. A. E. M. Janssen, 1994: *Dynamics and Modelling of Ocean Waves*. Cambridge University Press, 532 pp..

Lionello, P., P. Malguzzi, and A. Buzzi, 1998: Coupling between the atmospheric circulation and ocean wave field: An idealized case. *J.*

Phys. Oceanogr., **28,** 161–177.. Find this article online

Maat, N., C. Kraan, and W. A. Oost, 1991: The roughness of waves. *Bound.-Layer Meteor.*, **54,** 89–103..

Nordeng, T. E., 1991: On the wave age dependent drag coefficient and roughness length at sea. *J. Geophys. Res.*, **96,** 7167–7174..

Perrie, W., and L. Wang, 1995: A coupling mechanism for winds and waves. *J. Phys. Oceanogr.*, **25,** 615–630.. Find this article online

Smith, D. S., and Coauthors, 1992: Sea surface wind stress and drag coefficients: The HEXOS results. *Bound.-Layer Meteor.*, **60,** 109–142..

Snyder, R. L., F. W. Dobson, J. A. Elliot, and R. B. Long, 1981: Array measurements of atmospheric pressure fluctuations above surface gravity waves. *J. Fluid Mech.*, **102,** 1–59..

SWAMP Group, 1985: *Ocean Wave Modeling.* Plenum Press, 256 pp..

Toba, Y., N. Lida, H. Kawamura, N. Ebuchi, and I. S. F. Jones, 1990:Wave dependence of sea surface wind stress. *J. Phys. Oceanogr.*, **20,** 705–721.. Find this article online

Tolman, H. J., 1992: Effects of numerics on the physics in a third-generation wind-wave model. *J. Phys. Oceanogr.*, **22,** 1095–1111.. Find this article online

WAMDI Group, 1988: The WAM model—A third generation ocean wave prediction model. *J. Phys. Oceanogr.*, **18,** 1775–1810.. Find this article online

Weber, S., H. von Storch, P. Viterbo, and L. Zambresky, 1993: Coupling an ocean wave to an atmospheric general circulation model. *Climate Dyn.*, **9,** 63–69..

Wittmann, P. A., R. M. Clancy, and T. Metlach, 1995: Operational wave forecasting at Fleet Numerical Meteorology and Oceanography Center, Monterey, CA. Preprints, *Fourth Int. Workshop on Wave Hindcasting and Forecasting*, Banff, AB, Canada, Atmospheric Environment Service, 335–342..

Wu, J., 1980: Wind-stress coefficients over the sea surface during near neutral conditions—A revisit. *J. Phys. Oceanogr.*, **10,** 727–740.. Find this article online

Tables

Table 1. Locations of buoys used in model verification.

Buoy	Latitude (°N)	Longitude (°W)
41001	39.9	72.9
44005	42.6	68.6
44137	41.2	61.1
44138	44.2	53.6
44139	44.3	57.4
44141	42.1	56.2

Click on thumbnail for full-sized image.

Figures

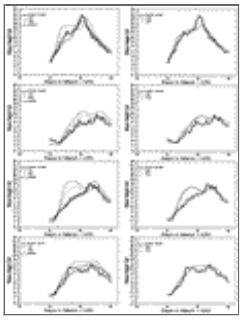

Click on thumbnail for full-sized image.

Fig. 1. Time series plots of SWH in meters at buoys 44137, 44138, 44139, and 44141 based on wave-induced stress τ_w (left panels) and wave age ξ (right panels). Solid lines indicate buoy observations, the dotted lines the SWH using the coupled

system, and the lines with the "+" symbol the SWH generated using the MMM wind in hindcast mode in a one-way interaction for wave-induced stress. The dashed lines are the SWH based on wave-induced stress using the uncoupled (left panels) and the coupled system (right panels).

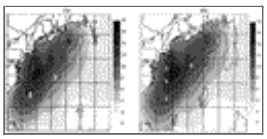

Click on thumbnail for full-sized image.

Fig. 2. WAM model-generated SWH in meters based on wave-induced stress (left panel) and wave age (right panel) valid at 1200 UTC 14 March 1993. The shaded regions are the SWH corresponding to coupled mode with the range of values for each shade of gray given by the vertical grayscale bar to the right. In (a) the superimposed contours with labels and central values are the SWH differences given as (CH − WS), while in (b) they are the SWH differences given as (CH − WA).

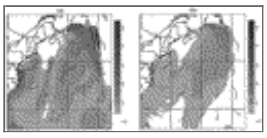

Click on thumbnail for full-sized image.

Fig. 3. WAM-generated Charnock parameter difference $\Delta\beta = (\beta - \beta_{CH}) \times 100$ valid 1200 UTC 14 March 1993 with $\beta_{CH} = 0.018$ and β the parameter communicated to the MC2 model. The vector wind field provided by the MC2 model to the WAM in the coupled mode is superimposed in meteorological convention with full barbs representing 10 m s^{-1} and half barbs 5 m s^{-1}. The left panel is for model run using WS and the right panel for that using WA in the coupled mode.

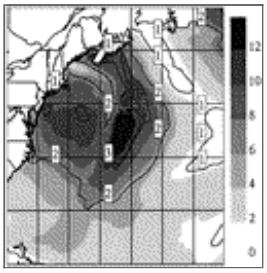

Click on thumbnail for full-sized image.

Fig. 4. The 24-h forecast of WAM-derived friction velocity × 10 (grayscale region) in m s^{-1} and drag coefficient × 1000 (solid line with labels and central values) based on WS for the coupled run valid at 1200 UTC 7 March 1986.

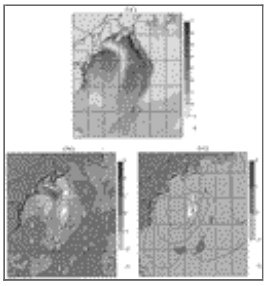

Click on thumbnail for full-sized image.

Fig. 5. The 24-h forecast of wave-generated parameters valid 1200 UTC 7 March 1986. In (a) the grayscale area shows the Charnock parameter differences $\Delta\beta$ = (coupled − uncoupled) × 100. In (b) the grayscale area is the same as (a) but for u_{10} in meters per second while the solid lines with labels and central values are u_{10} based on WS for the coupled run. (c) The same as (b) but for SWH in meters.

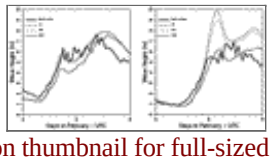

Click on thumbnail for full-sized image.

Fig. 6. Time series plots of the observed SWH and the SWH generated using the MC2 model winds based on three different sets of Charnock parameter at buoys 41001 and 44005. The solid lines are observed SWH, the dashed lines the SWH produced

by winds due to CH, the dotted lines the SWH produced by winds due to WS, and the lines with the "+" symbol the SWH produced by winds based on 5WS. See text for details.

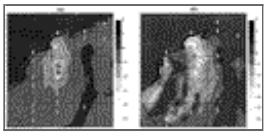

Click on thumbnail for full-sized image.

Fig. 7. The 24-h forecast of WAM-generated SWH in meters and u_* in meters per second valid at 0000 UTC 5 February 1995. In (a) the grayscale gives SWH differences (5WS − WS) in meters, while the black solid lines with labels and central values are WS. In (b) the grayscale and the solid lines are the same as in (a) but for u_*. See text for details.

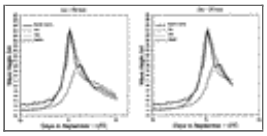

Click on thumbnail for full-sized image.

Fig. 8. Time series plots of SWH at buoy 44141 for two MC2 model grid resolutions: (a) 50 km and (b) 25 km. The solid lines give the observed SWH, the dashed lines the uncoupled SWH, the dotted lines the coupled SWH, and the lines with the "+" symbol the SWH generated using MMM winds in a hindcast mode.

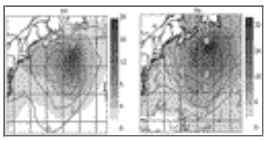

Click on thumbnail for full-sized image.

Fig. 9. The 24-h forecast/hindcast valid at 0000 UTC 11 September 1995 of (a) SWH in meters and (b) u_{10} in meters per second. The grayscale region gives the result based on MMM, while the solid lines with labels and central values are the result with coupling.

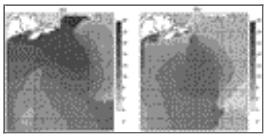

Click on thumbnail for full-sized image.

Fig. 10. The 24-h forecast/hindcast valid at 0000 UTC 11 September 1995 of WAM-generated peak periods in seconds of the dominant waves with the wind field in meteorological convention superimposed. A full barb represents 10 m s^{-1} and a half barb 5 m s^{-1}. In (a) the two fields correspond to the MMM winds, while in (b) the two fields correspond to the coupled winds.

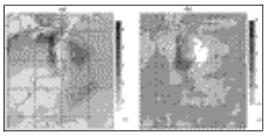

Click on thumbnail for full-sized image.

Fig. 11. The 24-h forecast valid at 0000 UTC 11 September 1995. In (a) the grayscale region gives $\Delta\beta$ = (coupled − uncoupled) × 100, solid lines the SWH differences (coupled − uncoupled) in meters, and the dashed lines the coupled swell height in meters. In (b) the grayscale region gives Δu_* = (coupled − uncoupled) in meters per second with the coupled vector wind field in meteorological convention superimposed. The barbs are as defined before.

Corresponding author address: Roop Lalbeharry, Recherche en Prévision Numérique, 4905 Dufferin Street, Downsview, ON M3H 5T4, Canada.

E-mail: Roop.Lalbeharry@ec.gc.ca